Original Article

Monte Carlo simulation and performance assessment of GE Discovery 690 VCT positron emission tomography/computed tomography scanner

ABSTRACT

The aim of this study is to simulate GE Discovery 690 VCT positron emission tomography/computed tomography (PET/CT) scanner using Geant4 Application for Tomographic Emission (GATE) simulation package (version 8). Then, we assess the performance of scanner by comparing measured and simulated parameter results. Detection system and geometry of PET scanner that consists of 13,824 LYSO crystals designed in 256 blocks and 24 ring detectors were modeled. In order to achieve a precise model, we verified scanner model. Validation was based on a comparison between simulation data and experimental results obtained with this scanner in the same situation. Parameters used for validation were sensitivity, spatial resolution, and contrast. Image quality assessment was done based on comparing the contrast recovery coefficient (CRC) of simulated and measured images. The findings demonstrate that the mean difference between simulated and measured sensitivity is <7%. The simulated spatial resolution agreed to within <5.5% of the measured values. Contrast results had a slight divergence within the range below 4%. The image quality validation study demonstrated an acceptable agreement in CRC for 8:1 and 2:1 source-to-background activity ratio. Validated performance parameters showed good agreement between experimental data and simulated results and demonstrated that GATE is a valid simulation tool for simulating this scanner model. The simulated model of this scanner can be used for future studies regarding optimization of image reconstruction algorithms and emission acquisition protocols.

Keywords: Digital phantom, Geant4 Application for Tomographic Emission, Monte Carlo simulation, positron emission tomography scanner, validation

Elham Kashian, Hadi Taleshi Ahangari[1], Vahab Dehlaghi, Karim Khoshgard[2], Pardis Ghafarian[3,4], Raheb Ghorbani[5]

Departments of Biomedical Engineering and Medical Physics and [2]Medical Physics, School of Medicine, Kermanshah University of Medical Sciences, Kermanshah, Departments of [1]Medical Physics and [5]Social Medicine, Faculty of medicine, Semnan University of Medical Sciences, Semnan, [3]Chronic Respiratory Diseases Research Center, National Research Institute of Tuberculosis and Lung Diseases (NRITLD), Shahid Beheshti University of Medical Sciences, [4]PET/CT and Cyclotron Center, Masih Daneshvari Hospital, Shahid Beheshti University of Medical Sciences, Tehran, Iran

Address for correspondence: Dr. Hadi Taleshi Ahangari, Department of Medical Physics, Faculty of Medicine, Semnan University of Medical Sciences, Semnan, Iran.
E-mail: taleshi@semums.ac.ir
Dr. Vahab Dehlaghi,
Department of Biomedical Engineering, Faculty of Medicine, Kermanshah University of Medical Sciences, Kermanshah, Iran.
E-mail: v.dehlaghi@kums.ac.ir

INTRODUCTION

Medical imaging modalities such as computed tomography (CT) and magnetic resonance imaging provide accurate anatomical information of the body by providing high spatial resolution and contrast. However, PET imaging, which is based on the body metabolism rate, does not offer a good spatial resolution despite its high sensitivity.[1,2] Given the constraints of each imaging system, multimodality systems such as PET/CT have been embraced and employed as a standard method for oncological staging and diagnosis.[3-5] Such systems can simultaneously provide anatomical and functional information of the body and high-resolution and high-sensitivity images,

Access this article online

Access this article online	
Website: www.wjnm.org	**Quick Response Code**
DOI: 10.4103/wjnm.WJNM_4_20	

in particular for therapeutic goals and precise determination of tumor volume.[6,7] The limitation of PET in terms of spatial resolution affects the image quality.[8] Therefore, several studies have focused on factors affecting PET image quality and spatial resolution, including photon noncollinearity, off-axis detector penetration, detector size and response, positron range, photon scatter, and patient motion, as well as the impact of each on improving the image quality.[9,10] Following these types of study in recent years, PET hardware and software have witnessed technological advancements, which have led to the ever-increasing enhancement of this scanner's performance.[10]

Several studies have used Monte Carlo methods to evaluate the parameters affecting image quality in nuclear medicine.[11] These methods are time-consuming, however, which have been relatively overcome with the advances in computer science and the advent of high-speed supercomputers, leading to their ever-increasing application particularly in PET and single photon emission computed tomography (SPECT) imaging.[12,13] Numerous Monte Carlo simulation codes have so far been developed, which are widely used in PET and SPECT imaging applications such as scanner design, image reconstruction, scatter correction, and imaging protocol enhancement.[14] SimSET, EGS4, MCNP,[15] and Geant4[16] are a number of such codes, which are precise and versatile and have been developed for physics with diagnostic and therapeutic energy.[17]

The Geant4 Application for Tomographic Emission (GATE) is a simulation code based on GEANT4 libraries and is a modular, versatile, and scripted toolkit specifically designed for nuclear medicine applications. This simulation code, developed by the International openGATE collaboration, allows defining time-dependent phenomena such as source decay time and source or patient movements.[5]

With the increased application of Monte Carlo simulations in research, validation studies are carried out to obtain accurate scanner models to be used in studies aiming at improving image quality and performance of imaging systems. Therefore, numerous validation studies have been conducted to determine the ability of various simulation codes, including the GATE, to model various scanners such as PET, neuroPET, small animal PET, and SPECT. Validation studies for PET scanners include the simulation of PET Allegro and GEMINI,[18] Advance/Discovery LS,[9] Biograph 2,[19] ECAT EXAT HR+,[20] Sedecal Argus preclinical PET,[21] FLEX Triumph™ preclinical PET/CT,[22] and rodent-research PET[8] scanners for small animals. Similar studies have been carried out on SPECT scanners.[23-25] Such studies have been occasionally conducted on multimodality scanners including PET/magnetic resonance[26] and PET/SPECT/CT.[27]

In the present study, the GATE simulation code was used for performance assessment and validation of the GE Discovery PET/CT 690 VCT scanner. This study aimed to provide an accurate and reliable model for this scanner and to evaluate its performance by a Monte Carlo simulator. This study aimed to design an accurate and reliable model of this scanner for the evaluation of performance parameters using GATE Monte Carlo simulation. Various validation studies were performed for numerous PET scanners. However, as per our knowledge, there are no such studies performed for the GE Discovery 690 scanner. However, the GE Discovery 690 scanner has not been validated so far, and the current study validates the simulation results of this scanner for the first time. In order to perform the simulation, the geometry, physics, and electronics of the device were defined by GATE. In addition to simulation, the scanner was used for imaging to achieve the gold standard required for validation. After performing the simulation and modification of its model, the experimental results from the scanner were compared with the simulation results in order to validate the designed model. The final analysis was limited to the comparison of the spatial resolution, sensitivity, and contrast of the simulation and experimental images. In addition, the image quality was evaluated. The results can be used in future studies for designing new PET scanners, optimization of acquisition protocols, development of reconstruction algorithms, and implementation of correction techniques to improve image quantification.

MATERIALS AND METHODS

Simulation
In this study, the GATE simulation package which is based on the Geant4 Monte Carlo simulation toolkit was used to simulate the PET scanner. This simulation code uses the Geant4 libraries and has a scripting mechanism. GATE has various modules, each assigned with the task of simulating a part of the scanner. These modules simulate the behavior of the system geometry, radioactive source, physics of interactions, scanner detectors, and signal processing chain to obtain a precise model of the desired system.

In this study, in order to simulate the PET/CT imaging system, the system geometry, physics processes, and signal flow, called the "digitizer" in GATE, were defined for the PET scanner in the simulation code and will be explained in detail:

Geometry
In GATE, simple geometries such as cylinder, box, and sphere can be defined. These geometries can be used and combined to produce any other kind of geometry, even complex geometries. In this study, the geometry of the PET scanner detectors and its shields were defined in detail.

The GE Discovery 690 VCT PET scanner system has 13,824 LYSO crystals with dimensions of 4.2 mm × 6.3 mm × 25 mm, arranged in 24 ring detectors. The detection unit of this scanner is composed of blocks consisting of 9 × 6 crystals, each containing a total of 64 blocks per ring. The geometry branch was used to model ring detectors consisting of blocks and crystals. In addition, the shields surrounding the scanner rings and the light guides around the crystals were also defined to incorporate the photon scattering media into the model [Figure 1].

Physics

Physics in GATE is based on GEANT4 libraries, which include physical models of all interactions for particles and photon with different energies. In this simulation, the standard model was defined for photonic interactions (photoelectric, compton, ionization, and bremsstrahlung) and the PENELOPE model for the Rayleigh interactions;[27] the energy cutoff of

Figure 1: Schematic representation of the Discovery 690 positron emission tomography scanner model with its ring shields simulated using Geant4 Application for Tomographic Emission (a), including oblique view of a block (b) and a crystal (c)

photons and electrons was considered 1 cm for LYSO crystals and 10 cm for the phantom.

Signal processing

Digitizer, which simulates the behavior of the electronic components and the signal processing of the scanner, is one of the most vital parts of the GATE simulation for achieving a real, reasonable, and comparable output. Digitizer has different modules that mimic each part of the signal processing chain, and the presence, absence, or change in each module can lead to a fundamental change in the final output. Therefore, defining this part is so important in imaging scanners. The defined layout of the digitizer in this study is shown in Figure 2.

A sequence of modules was used to model the digitizer. The Geant4 hits module, which imitates the production of photons due to the interaction of gamma rays with detector crystals, is the first step in defining the signal-processing chain. Subsequently, the Adder module was placed. The Adder collects the energy deposited by hits and stores time information with respect to the last recorded interaction and site by weighing the energy deposited by particles. The readout module was then defined, which collects the previous module information at a larger level from the detector, i.e., the blocks, and generates the pulse. Energy blurring is the next module, which simulates the readout of the produced pulse energy spectrum blur. The scanner crystal is made of LYSO. In some studies, a constant energy resolution for this type of crystal has been defined.[18,28] In fact, the energy resolution of all crystals is not the same; therefore, the energy resolution of the crystals was determined using the crystal blurring module in a nonuniform range of 10% and 20%. The
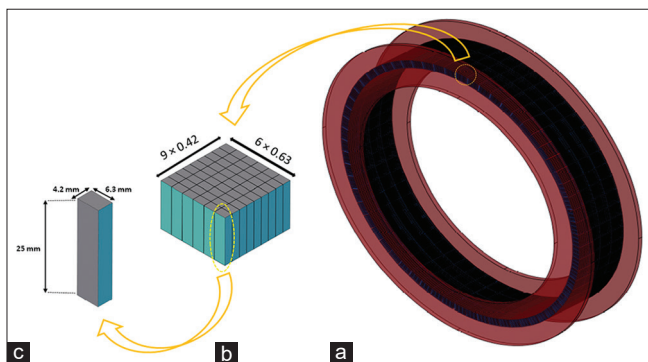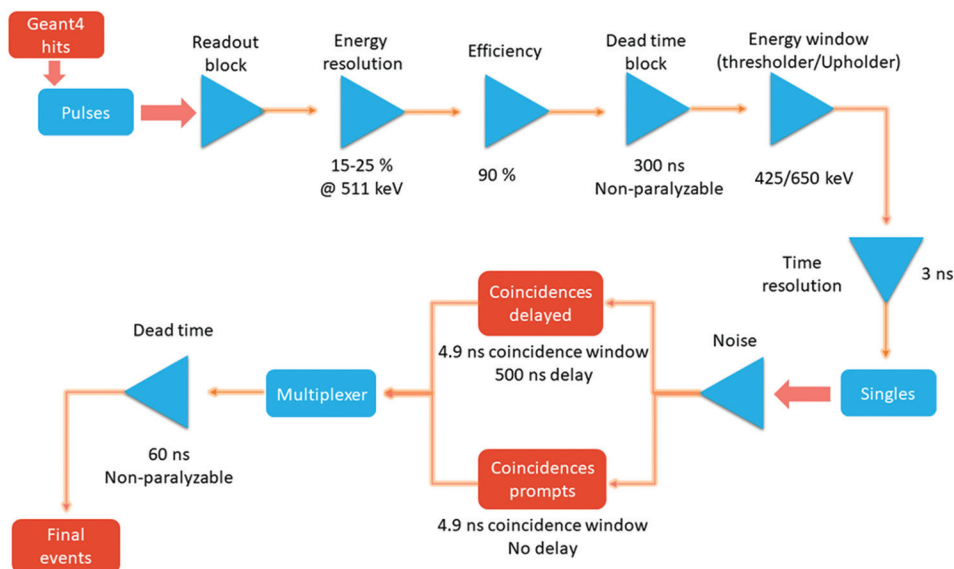

Figure 2: Flowchart display of digitizer module of Discovery 690 positron emission tomography scanner

detection efficiency factor, equal to 90%, was also applied to the readout output.[29,30] In addition, the time blurring module was applied to the recorded singles with a temporal resolution of 3 ns. The resolution value was defined according to the value considered by Stortz *et al.*,[31] who used a similar detector to what was used in the present study (LYSO). Simulation of the dead-time effect on the detection of events was performed using the dead-time module. Since Eriksson *et al.*[32] showed that two paralyzable dead-time (one at the level of the singles and the other at the coincidence level) is enough to emulate the count rate performance in the PET scanner, the effect of dead-time was also considered in this simulation at the stage of recording singles in scintillation detectors and at the stage of recording coincident event in electronic circuits. The dead-time module of 300 ns was applied at block levels and 60 ns at the coincidence recording stage. In order to reduce the scattering effect, the energy window in the range of 425–650 keV was then determined in accordance with the vendor's recommendation for a standard device function. This section was applied to the dead-time output singles by the thresholder and upholder modules. In the next step, the singles were investigated in terms of coincident events. Coincidence occurs when two singles are recorded with a relatively similar energy at a range of 511 keV in a time window in two detectors apart from each other. To define this part in the GATE, a coincidence module with a 4.9 ns time window was defined, and a 4.9 ns delay time window with a 500 ns offset was used for the estimation of the random events. The coincidence dead-time mentioned above was included in this section. Crystal crosstalk effects and pileup rejection were not considered in this simulation as the information needed to model these two effects is not readily available. Ignoring these effects in simulation may influence the simulation results and lead to different simulation and experimental results. The parameters defined for simulating the scanner signal processing chain, including energy resolution, energy window, coincidence time window, and delay time windows for collection of random events, were extracted from the datasheet published by the manufacturer and from the study of Bettinardi *et al.*[10]

Assessment strategy
Model verification
After simulating the scanner, four line sources, with a diameter of 1.1 mm and a length of 75 mm which were, respectively, placed at the center, and 1, 10, and 20 cm tangentially from the center of field of view (FOV), were used to evaluate the simulated scanner model. Figure 3 depicts the position of the simulated line sources. The Full width at half maximum (FWHM) of the line spread function was then calculated in simulation and experimental images by interpolation between adjacent pixels. In addition, the sensitivity of the center of FOV was
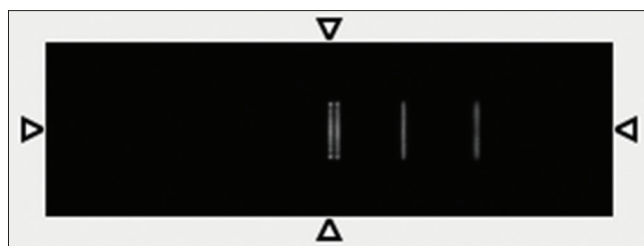

Figure 3: Illustration of simulated line sources placed at the center of field of view and 1, 10, and 20 cm tangentially from the center of field of view showed in the A Medical Image Data Examiner

calculated in all slices, and the sensitivity diagram was plotted as a function of the image slice number in order to examine the model correctness. Finally, based on the comparison results, the simulation parameters were modified to allow the simulation results to approach the experimental results, offering a precise model of the scanner.

Model validation
Voxelized phantom – A polymethyl methacrylate-made phantom with a height of 30 cm and a diameter of 19 cm was used for the experimental part of validation. In this phantom, eight cylinders of 8, 11, 16, and 21 mm in eight different positions in the active FOV were placed and filled uniformly with water and F^{18}. The activity level used for the background was 3.54 Bq/cc. Each source had two different activity concentrations, i.e., two times and eight times of the background activity, in two different positions. Figure 4 shows the cylindrical phantom used in this study.

The experimental measurements were carried out at the Tehran MassihDaneshvari Hospital using the GE Discovery 690 VCT PET/CT scanner. The voxelized phantom module of the GATE was used to simulate the phantom. To this end, a $256 \times 256 \times 12$ matrix was assigned to the phantom, and a phantom with similar dimensions to the experimental phantom was designed therein. The activity concentration and tissue attenuation per pixel corresponding to the clinic were then defined in two ASCII files, i.e., activity and attenuation. Instead of defining the positron emitter source, the back-to-back gamma source was defined during simulation. The GATE code was validated by comparing the measured and the simulated images in terms of the three parameters of spatial resolution, sensitivity, and contrast.

The simulation output data were reconstructed using Software for Tomographic Image Reconstruction (STIR),[33] and ECAT7 output was used to reconstruct the image with STIR. The implemented reconstruction algorithm was OSEM. Images with a $256 \times 256 \times 12$ matrix were reconstructed. The output data were not corrected in terms of attenuation, normalization, and noncollinearity.

Spatial resolution

In this study, the spatial resolution was calculated for four sources with an activity eight times that of the background with different dimensions and positions. These sources were placed in four different positions from the center (radially and tangentially 7 cm apart from the center of FOV).

The spatial resolution of all sources was obtained in two axial positions, i.e., the central and ¼ axial FOV slice, by determining FWHM for point spread function, through interpolation between the adjacent pixels in the radial and tangential profiles.

Sensitivity

At this stage, the region of interest (ROI) was plotted in the source range and in a similar-sized range in the background. The accumulated counts were then calculated in these ROIs. To calculate the count rate, the count values were divided by the imaging time. The sensitivity was then calculated using the count rates of sources and the corresponding backgrounds, as well as the activity of each source, according to the following formula:

$$S = \frac{R_S - R_{BG}}{A_S}$$

Where R_s is the source count rate, R_{BG} is the background count rate, and A_S is the source activity.

Contrast

In order to evaluate the image contrast, several ROIs were plotted on the sources and on the image uniform regions, as the background in the central slice. The contrast was then calculated according to the following equation:

$$Contrast = \frac{C_S}{C_{BG}}$$

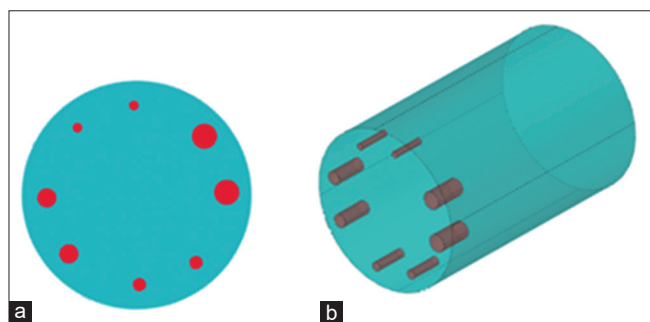Where C_S is the mean source count and C_{BG} is the mean background count.

Figure 4: Graphical illustration of cylindrical validation phantom. Top (a) and oblique (b) views

Image quality

The CRC was used to evaluate the image quality. This parameter was measured in two source-to-background ratios of 2:1 and 8:1 for a slice at the center in four different positions. First, the source and background counts were calculated by drawing several ROIs for the sources and the background. Then, using the source-to-background ratio and the calculated count, the CRC was calculated as follows:

$$CRC = \frac{\dfrac{N_S}{N_{BG}} - 1}{\dfrac{A_S}{A_{BG}} - 1} \times 100$$

Where N_S and N_{BG} are the mean source and background counts, respectively, and A_S and A_{BG} are the source and background activity concentrations, respectively.

RESULTS

Model verification

Table 1 presents the results of FWHM for evaluation of the simulation accuracy and optimization of simulation parameters in the measured and simulated images for four line sources in millimeters.

In Figure 5, the FWHM diagram of the line sources is represented as a function of the spatial position. According to the diagram, the image FWHM increases by increasing the distance from the FOV center in two simulated and measured images. The process of FWHM changes is similar in two simulated and clinical images.

Figure 6 qualitatively examines the trend of sensitivity changes in two simulated and experimental images. This diagram shows the sensitivity at the center of FOV, which is the location of a line source. The diagram demonstrates that the sensitivity is high in the line source range and tends to zero outside the line source where there is no activity. The qualitative examination of this diagram shows that simulation and experimental results have similar trends.

Table 1: Measured FWHM for sources in different positions tangentially from the center: Simulated and experimental results

Line source position tangentially from the center (cm)	Measured values (mm)	Simulated values (mm)
20	1.30	1.71
10	1.20	1.53
1	1.15	1.46
0 (center)	1.15	1.45

FWHM: Full width at half maximum

Model validation
Spatial resolution
The images for the quantification of the spatial resolution were reconstructed using the STIR and OSMAPOSLcode without normalization correction. FWHM calculations were performed on both clinical and simulated images. The spatial resolution was calculated radially and tangentially in millimeters in each of the four positions related to cylindrical sources in the central and ¼ axial FOV slice; the results are reported in Tables 2 and 3. The differences between simulated and measured values are also specified in the last column. Based on the findings, the results of the simulation spatial resolution had a mean difference, with the measured values, of <6.5% in the tangential direction and <5.5% in the radial direction.

Figure 7 depicts the FWHM changes in terms of source dimensions. Based on this chart, the spatial resolution decreases by increasing the source diameter. This trend was observed in both simulation and experimental images for both central and ¼ axial FOV slices.

Sensitivity
Table 4 compares the sensitivity values in four different positions for the scanner and simulated images in two central and ¼ axial FOV slices. The sensitivity values are in cps.kBq^{-1}. According to the results reported in this table, the mean sensitivity difference in the simulation image was <7% compared to the experimental results.

Contrast
In Table 5, the contrast results are reported for sources with different dimensions and different positions in the two source-to-background ratios. As expected, the sources' contrast in the 2:1 source-to-background ratio was less than

the 8:1 source-to-background ratio, which was observed in both the simulated and measured images.

Figure 8a and b illustrates the sources' contrast as a function of the source diameter for the source-to-background ratio of 2:1 and 8:1. As shown in these diagrams, the contrast is

Table 2: Tangential simulated and measured FWHM for sources in different positions in central and 1/4 axial field of view slice

Source position measured axially from the center	Measured values (mm)	Simulated values (mm)	Difference (%)
Center of FOV			
Tangential (right)	6.050	5.16	14.7
Tangential (left)	4.465	4.08	8.6
Radial (down)	3.670	3.60	1.9
Radial (up)	3.020	2.85	5.6
1/4 of FOV			
Tangential (right)	6.040	5.655	6.4
Tangential (left)	4.400	4.005	9
Radial (down)	3.695	3.25	12
Radial (up)	3.18	3.1	2.5

FOV: Field of view; FWHM: Full width at half maximum

Table 3: Radial simulated and measured FWHM for sources in different position in central and 1/4 axial field of view slice

Source position measured axially from the center	Measured values (mm)	Simulated values (mm)	Difference (%)
Center of FOV			
Tangential (right)	6.060	6.005	0.9
Tangential (left)	4.515	4.38	3
Radial (down)	3.370	3.285	2.5
Radial (up)	2.930	2.53	13.6
1/4 of FOV			
Tangential (right)	6.1	5.975	2.05
Tangential (left)	4.52	4.31	4.65
Radial (down)	3.35	3.29	1.8
Radial (up)	2.885	2.525	12.5

FOV: Field of view; FWHM: Full width at half maximum
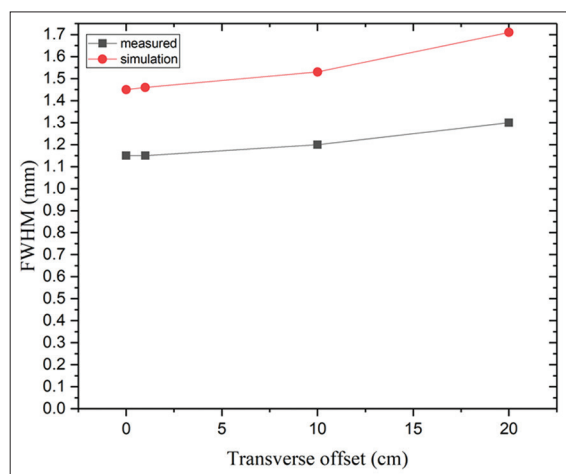
Figure 5: The full width at half maximum as a function of tangential placement of sources. Results for central slice of simulated and measured images
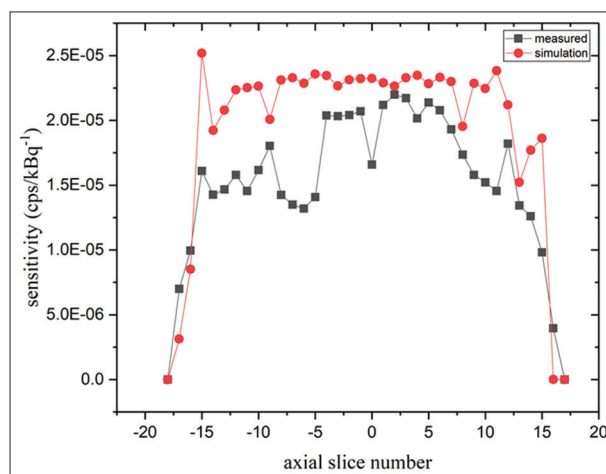
Figure 6: Sensitivity as a function axial slice number at the center of field of view. Results for simulated and measured images

increased by increasing the source size in both simulated and clinical images.

Image quality

The simulation output was reconstructed using STIR and the OSMAPOSL code in order to evaluate the quality of simulated images. Then, the CRC was calculated for both clinical and simulated images. The results of these calculations are reported in Table 6, according to which, the

mean difference of the simulation image recovery coefficient was below 8%.

The two diagrams of Figure 9 show the CRC percent for the simulated and measured data, and diagrams a and b represent CRC for the 2:1 and 8:1 source-to-background ratios, respectively. These diagrams compare the image contrast for the sources with four different sizes. As can be seen, there is a good agreement between the simulated and measured values in each of the four sizes. According to the diagrams, in both source-to-background ratios, CRC increases with the increase in the sources' diameter, which is evident in both simulated and experimental images.

DISCUSSION

The present study aimed to develop an accurate model of the GE Discovery 690 PET scanner and evaluate its performance using the GATE Monte Carlo simulation. The validity of the proposed model was also evaluated against experimental data.

In the first stage, the scanner was simulated. To this end, its geometry was designed in the GATE simulation code

Table 4: Simulated and measured sensitivity for sources in different positions in central and 1/4 axial field of view slice

Source position measured axially from the center	Measured values (×10⁻³ cps/kBq)	Simulated values (×10⁻³ cps/kBq)	Difference (%)
Center of FOV			
Tangential (right)	1.49	1.39	7.11
Tangential (left)	1.46	1.37	6.33
Radial (down)	1.45	1.35	7.01
Radial (up)	1.23	1.12	9.21
1/4 of FOV			
Tangential (right)	1.43	1.33	6.77
Tangential (left)	1.47	1.35	8.5
Radial (down)	1.40	1.37	1.77
Radial (up)	1.21	1.34	9.99

FOV: Field of view

Table 5: Comparison between simulated and experimental values obtained for the contrast of four sources with different size in two different source-to-background ratios

Source position measured axially from the center	Source diameter (mm)	Measured values (%)	Simulated values (%)	Difference (%)
Source-to-background ratio 2:1				
Tangential (right)	21	1.73	1.72	0.42
Tangential (left)	16	1.67	1.63	2.2
Radial (down)	11	1.30	1.32	2.16
Radial (up)	8	1.17	1.16	1.44
Source-to-background ratio 8:1				
Tangential (right)	21	4.8	4.88	1.98
Tangential (left)	16	4.15	4.53	5.7
Radial (down)	11	3.53	3.35	5.7
Radial (up)	8	2.43	2.23	10.85
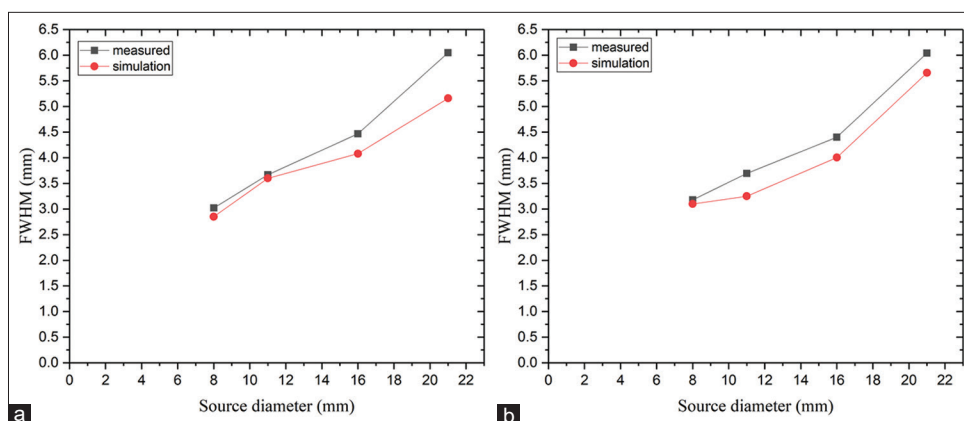
Figure 7: Simulated and measured tangential FWHM as a function of source diameter in central (a) and ¼ axial field of views (b)
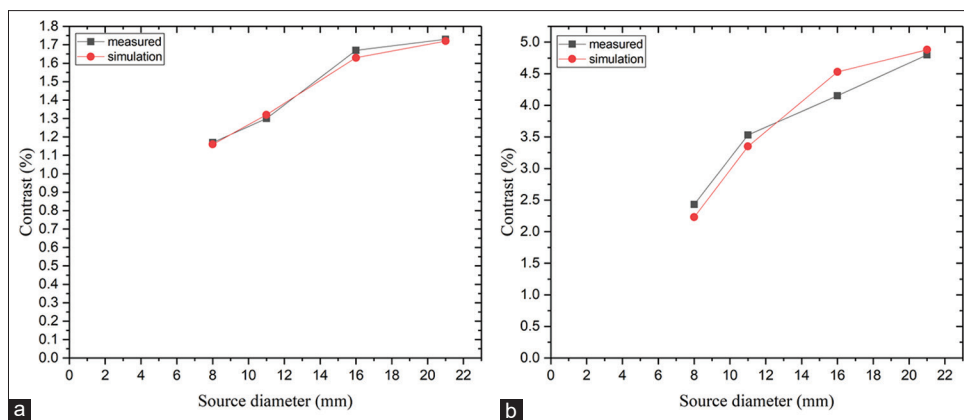
Figure 8: Contrast of four sources with 2:1 (a) 8:1 (b) source-to-background ratios. The plots refer to simulated and measured images
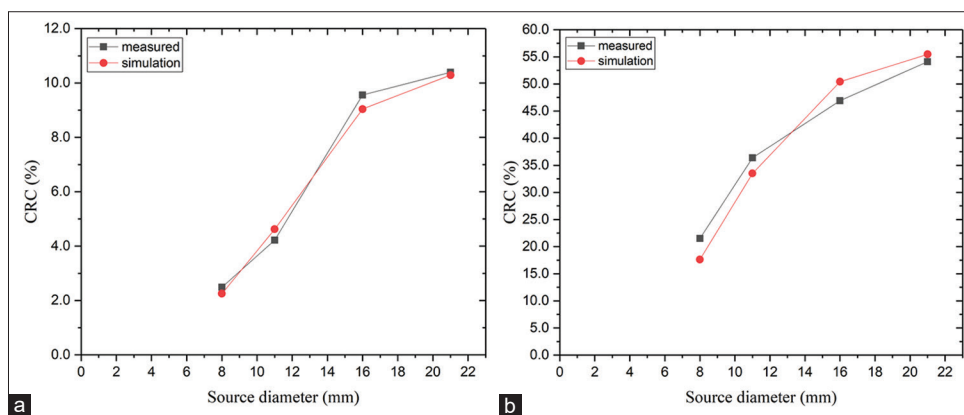

Figure 9: Contrast recovery coefficient calculated over region of interests in central slice encompassing the four sources in cylindrical phantom as a function of source diameter. The plots refer to images with source-to-background ratio 2:1 (a) and 8:1 (b)

Table 6: Comparison between simulated and experimental values obtained for the contrast recovery coefficient of four sources with different size in two different source-to-background ratios

Source position measured axially from the center	Source diameter (mm)	Measured values (%)	Simulated values (%)	Difference (%)
Source-to-background ratio 2:1				
Tangential (right)	21	10.39	10.29	0.96
Tangential (left)	16	9.56	9.04	5.44
Radial (down)	11	4.22	4.62	9.48
Radial (up)	8	2.49	2.25	9.64
Source-to-background ratio 8:1				
Tangential (right)	21	54.10	55.46	2.51
Tangential (left)	16	46.91	50.40	7.44
Radial (down)	11	36.39	33.50	7.94
Radial (up)	8	21.50	17.62	18.05

based on the information from the scanner geometry. The physics of interactions was then defined. The digitizer, which mimicked the scanner signal flow, was simulated based on the specifications of the scanner and information from the device provided by the manufacturer. After system simulation, the accuracy of the developed model was evaluated using the line sources and comparing the scanner images with the simulated images. The results of simulation and measured data were approached through modification of the digitizer module parameters, and a model with an

acceptable correctness was presented. In order to validate the developed model, the voxelized phantom was used by performing the validation with an emphasis on the sensitivity, spatial resolution, and contrast of the images. The CRC parameter was compared in two images in order to evaluate the simulated image quality.

The spatial resolution of the line sources in Figure 5 indicates that the spatial resolution decreases with an increase in the source distance from the center, which is consistent with the

results reported by Grogg *et al*.[34] This decrease in spatial resolution can be influenced by the detector geometric factors, such as depth of interaction, that can be observed both in simulation and measured data. The similar trend of FWHM variations in this diagram in both simulation and experimental modes confirms the correctness of the proposed model. The observed difference between simulation and experimental results is due to a number of phenomena that basically occur during the radiation detection and image formation processes. However, they were not considered in the current simulation due to lack of access to the exact information required for their simulation. Therefore, in future studies, a scale factor can be obtained and applied to the simulation results to improve the accuracy of the proposed model and reduce the impact of these phenomena.

Quantitative evaluation of the image sensitivity, as a function of the slice number [Figure 6], indicates that the sensitivity variation trend was correct with respect to the presence of a line source in the study area in both the simulated and measured images, and a sensitivity peak existed in the system center, precisely in the region of the line sources. This sensitivity was sharply reduced in the area outside the line source length. Nonuniform variations of the sensitivity in the original image can be due to the fact that the central line source was not at a flat and stable position during imaging, affecting the sensitivity results as the count accumulated from each area as per the activity concentration. However, the similar trend to the results confirms the correctness of the simulation and the proposed model.

Tables 2 and 3 show a good agreement between the simulated and experimental spatial resolution results in both radial and tangential directions. The simulated radial and tangential FWHM values had a mean difference of <6.5% compared to the experimental values. This means that the spatial resolution of simulated images was better than the measured images. This underestimation for FWHM can be attributed to nonsimulation of a number of phenomena in the GATE. For example, light shielding between and inside block detectors as well as the inherent limitation of photo multiplier tube (PMTs) and optical scattering occurring in crystals was not considered. In addition, the light sharing between PMTs can also be specified as a reason,[35] which was not considered in this simulation. Simulation of the crosstalk phenomenon between crystals can also reduce the difference between results. The evaluation of spatial resolution in Figure 7 illustrates the relationship between the source size and FWHM, meaning that the spatial resolution decreases by increasing source dimensions. This problem can be similarly observed in both the simulated and experimental images.

The mean overall difference between the simulated and measured sensitivity results was <7%, which is acceptable. This difference can be attributed to the factors described for the spatial resolution. The definition of a global quantum efficiency in this study has an impressive effect on reducing the difference between results. However, considering a uniform quantum efficiency is consistent with the reality. Therefore, taking into account a variable quantum efficiency can greatly reduce these disparities.

According to Table 5, the simulated image contrast for the two source-to-background ratios of 2:1 and 8:1 had a mean divergence of 1.5% and 6%, respectively. The results show a good agreement in the contrast between the simulated and measured images. As expected, with increasing the source diameter, the image contrast increases. The contrast in the source-to-background ratio of 8:1 was more than 2:1, which was observed in both simulated and experimental images [Figure 8].

Based on what is reported in Table 6, the CRC results show a good agreement between the simulated and clinical images, and the mean difference in results for the source-to-background ratio of 2:1 and 8:1 was <6.5% and 9%, respectively. Comparison of the CRC results for evaluation of image quality indicated that the divergence of results was higher for sources with smaller diameter. This conclusion was also reported in the Zagni *et al.*'s study.[18] Figure 9 shows that in both source-to-background ratios of 2:1 and 8:1, the higher the diameter of the source, the higher will be the CRC; this is consistent with the data published in other studies.

In general, the observed differences in the results were in an acceptable range, and these under- and over-estimations can be related to the effects of the actual detection process mentioned earlier and to the inaccessibility to precise information for their definition in GATE. In addition, the model proposed in this study was simulated based on finite geometric information of scanner geometry, and hence was approximate.

CONCLUSION

In this study, the performance parameters of the GE Discovery 690 PET scanner were evaluated using GATE MC simulation and validated with the results obtained from clinical images. The spatial resolution, sensitivity, contrast, and image quality evaluated for the scanner in this study are well validated. Furthermore, the results indicate that the designed model has potential to become a reliable tool for imaging protocol optimization, design of new scanners, and performance evaluation under different imaging conditions.

Conflicts of interest

There are no conflicts of interest.

REFERENCES

1. Foster B, Bagci U, Mansoor A, Xu Z, Mollura DJ. A review on segmentation of positron emission tomography images. Comput Biol Med 2014;50:76-96.

2. Bagci U, Udupa JK, Mendhiratta N, Foster B, Xu Z, Yao J, *et al*. Joint segmentation of anatomical and functional images: Applications in quantification of lesions from PET, PET-CT, MRI-PET, and MRI-PET-CT images. Med Image Anal 2013;17:929-45.

3. MacManus M, Nestle U, Rosenzweig KE, Carrio I, Messa C, Belohlavek O, *et al*. Use of PET and PET/CT for radiation therapy planning: IAEA expert report 2006-2007. Radiother Oncol 2009;91:85-94.

4. Kinahan PE, Doot RK, Wanner-Roybal M, Bidaut LM, Armato SG, Meyer CR, *et al*. PET/CT assessment of response to therapy: Tumor change measurement, truth data, and error. Transl Oncol 2009;2:223-30.

5. Jan S, Santin G, Strul D, Staelens S, Assié K, Autret D, *et al*. GATE: A simulation toolkit for PET and SPECT. Phys Med Biol 2004;49:4543-61.

6. Yu K, Chen X, Shi F, Zhu W, Zhang B, Xiang D. A novel 3D graph cut based co-segmentation of lung tumor on PET-CT images with Gaussian mixture models. In medical imaging 2016: Image processing. Int Soc Optics Photonics 2016;9784:97842V.

7. Bagci U, Udupa JK, Yao J, Mollura DJ. Co-segmentation of functional and anatomical images. Med Image Comput Comput Assist Interv 2012;15:459-67.

8. Baghaei H, Zhang Y, Li H, Wang Y, Kim S, Ramirez RA, *et al*. GATE Monte Carlo simulation of a high-sensitivity and high-resolution LSO-based small animal PET camera. IEEE Trans Nucl Sci 2007;54:1568-73.

9. Schmidtlein CR, Kirov AS, Nehmeh SA, Erdi YE, Humm JL, Amols HI, *et al*. Validation of GATE Monte Carlo simulations of the GE Advance/ Discovery LS PET scanners. Med Phys 2006;33:198-208.

10. Bettinardi V, Presotto L, Rapisarda E, Picchio M, Gianolli L, Gilardi MC. Physical performance of the new hybrid PET∕CT Discovery-690. Med Phys 2011;38:5394-411.

11. Ljungberg M, Strand SE, King MA. Monte Carlo Calculations in Nuclear Medicine: Applications in Diagnostic Imaging. United Satates: CRC Press; 2012. p. 278-312.

12. Zaidi H. Relevance of accurate Monte Carlo modeling in nuclear medical imaging. Med Phys 1999;26:574-608.

13. Buvat I, Castiglioni I. Monte Carlo simulations in SPET and PET. Q J Nucl Med 2002;46:48-61.

14. Strulab D, Santin G, Lazaro D, Breton V, Morel C. GATE (Geant4 application for tomographic emission): A PET/SPECT general-purpose simulation platform. Nucl Phys B 2003;125:75-9.

15. Waters LS. MCNPX User's Manual. United States: Los Alamos National Laboratory; 2002. p 1-5.

16. Agostinelli S, Allison J, Amako Ka, Apostolakis J, Araujo H, Arce P, *et al*. EANT4 – A simulation toolkit. Nucl Instrum Methods Phys Res A 2003;506:250-303.

17. Assie K, Breton V, Buvat I, Comtat C, Jan S, Krieguer M, *et al*. Monte Carlo simulation in PET and SPECT instrumentation using GATE. Nucl Instrum Methods Phys Res A 2004;527:180-9.

18. Lamare F, Turzo A, Bizais Y, Le Rest CC, Visvikis D. Validation of a Monte Carlo simulation of the Philips Allegro/GEMINI PET systems using GATE. Phys Med Biol 2006;51:943-62.

19. Nikolopoulos D, Michail C, Valais I, Yannakopoulos P, Kottou S, Karpetas G, *et al*. GATE simulation of the biograph 2 PET/CT scanner. J Nucl Med Radiat Ther 2014;5:2.

20. Jan S, Comtat C, Strul D, Santin G, Trebossen R. Monte Carlo simulation for the ECAT EXACT HR+ system using GATE. IEEE Trans Nucl Sci 2005;52:627-33.

21. Zagni F, D'Ambrosio D, Spinelli AE, Cicoria G, Fanti S, Marengo M. Accurate modeling of a DOI capable small animal PET scanner using GATE. Appl Radiat Isot 2013;75:105-14.

22. Zeraatkar N, Ay MR, Kamali-Asl AR, Zaidi H. Accurate Monte Carlo modeling and performance assessment of the X-PET subsystem of the FLEX triumph preclinical PET/CT scanner. Med Phys 2011;38:1217-25.

23. Staelens S, Strul D, Santin G, Vandenberghe S, Koole M, D'Asseler Y, *et al*. Monte Carlo simulations of a scintillation camera using GATE: Validation and application modelling. Phys Med Biol 2003;48:3021-42.

24. Sakellios N, Rubio JL, Karakatsanis N, Kontaxakis G, Loudos G, Santos A, *et al*. GATE simulations for small animal SPECT/PET using voxelized phantoms and rotating-head detectors. IEEE Nucl Sci Symp Conf Rec 2006;4:2000-3.

25. Vieira L, Vaz TF, Costa DC, Almeida P. Monte Carlo simulation of the basic features of the GE Millennium MG single photon emission computed tomography gamma camera. Rev Esp Med Nucl Imagen Mol 2014;33:6-13.

26. Aklan B, Jakoby BW, Watson CC, Braun H, Ritt P, Quick HH. GATE Monte Carlo simulations for variations of an integrated PET/MR hybrid imaging system based on the Biograph mMR model. Phys Med Biol 2015;60:4731-52.

27. Lee S, Gregor J, Osborne D. Development and validation of a complete GATE model of the Siemens Inveon trimodal imaging platform. Mol Imaging 2013;12:1-3.

28. Karakatsanis N, Sakellios N, Tsantilas N, Dikaios N, Tsoumpas C, Lazaro D, *et al*. Comparative evaluation of two commercial PET scanners, ECAT EXACT HR+ and Biograph 2, using GATE. Nucl Instrum Methods Phys Res A 2006;569:368-72.

29. Lecoq P, Gektin A, Korzhik M. Inorganic Scintillators for Detector Systems: Physical Principles and Crystal Engineering. Switzerland: Springer; 2016. p. 175-92.

30. van Eijk CW. Inorganic scintillators in medical imaging. Phys Med Biol 2002;47:R85-106.

31. Stortz G, Walker M, Thompson C, Goertzen A, Retiere F, Zhang X, *et al*. Characterization of a new MR compatible small animal PET scanner using Monte-Carlo simulations. IEEE Trans Nucl Sci 2013;60:1637-44.

32. Eriksson L, Wienhard K, Dahlbom M. A simple data loss model for positron camera systems. IEEE Trans Nucl Sci 1994;41:1566-70.

33. Thielemans K, Tsoumpas C, Mustafovic S, Beisel T, Aguiar P, Dikaios N, *et al*. STIR: Software for tomographic image reconstruction release 2. Phys Med Biol 2012;57:867-83.

34. Grogg KS, Toole T, Ouyang J, Zhu X, Normandin MD, Li Q, *et al*. National electrical Manufacturers association and clinical evaluation of a novel brain PET/CT scanner. J Nucl Med 2016;57:646-52.

35. Wilson DW, Furenlid LR, Barrett HH, Chen YC. A new PET system for small-animal imaging. IEEE Nucl Sci Symp Conf Rec (1997) 2004;6:3389-92.